A COMBINED EXPERIMENTAL AND NUMERICAL APPROACH TO THE ASSESSMENT OF FLOC SETTLING VELOCITY USING FRACTAL GEOMETRY

R. B. Moruzzi[a*], J. Bridgeman[b], P.A.G. Silva[a]

a – UNESP - Univ Estadual Paulista, Instituto de Geociências e Ciências Exatas, Brazil

b – Faculty of Engineering & Informatics, University of Bradford, United Kingdom

Address:

* Corresponding author: Avenida 24-A, nº 1515, C. P. 178, CEP 13506-900, Bela Vista, Rio Claro, São Paulo, Brazil. Phone: +55 19 3526-9339. *E-mail address*: rodrigo.moruzzi@unesp.br

Abstract

Sedimentation processes are fundamental to solids / liquid separation in water and wastewater treatment, and therefore a robust understanding of the settlement characteristics of mass fractal aggregates (flocs) formed in the flocculation stage is fundamental to optimized settlement tank design and operation. However, the use of settling as a technique to determine aggregates' traits is limited by current understanding of permeability. In this paper, we combine experimental and numerical approach to assess settling velocities of fractal aggregates. Using a non-intrusive in situ digital image-based method, three and two-dimensional fractal dimensions were calculated for kaolin-based flocs. By considering shape and fractal dimension, the porosity, density and settling velocities of the flocs were calculated individually, and settling velocities compared to those of spheres of the same density using Stokes' law.

Shape analysis shows that the settling velocities for fractal aggregates may be greater or less than those for perfect spheres. For example, fractal aggregates with floc fractal dimension, D_f = 2.61, floc size, d_f > 320 μm and d_p = 7.5 μm settle with lower velocities than those predicted by Stokes' law; whilst, for D_f = 2.33, all aggregates of d_f > 70 μm and d_p = 7.5 μm settled below the velocity calculated by Stokes' law for spheres. Conversely, fractal settling velocities were higher than spheres for all range of sizes, when D_f of 2.83 was simulated. The ratio of fractal aggregate to sphere settling velocity (the former being obtained from fractal porosity and density considerations), varied from 0.16 to 4.11 for aggregates in the range of 10 and 1000 μm, primary particle size of 7.5 μm and a three-dimensional fractal dimension between 2.33 and 2.83. However, the ratio decreases to the range of 0.04 to 2.92, when primary particle size changes to 1.0 μm for the same fractal dimensions.

Using the floc analysis technique developed here, the results demonstrate the difference in settlement behaviour between the approach developed here and the traditional Stokes' law approach using solid spheres. The technique and results demonstrate the improvements in understanding, and hence value to be derived from an analysis based on fractal, rather than Euclidean, geometry when considering flocculation and subsequent clarification performance.

Keywords: flocculation, fractal dimension, settling velocity, porosity, density

Introduction

Coagulation and flocculation are critical steps in drinking water treatment. During coagulation, a coagulant (e.g. aluminium sulphate) is added to the water to neutralize the negatively charged suspended particles, following which shear-induced interactions generated by slow mixing in a flocculator cause their aggregation into mass fractal aggregates (flocs). Clarification processes in water treatment are often based on sedimentation of flocs. In order to optimise sedimentation, it is important to gain a fundamental understanding of floc settling behaviour. Traditional approaches have used Stokes' law with its inherent assumptions of solid, spherical particles. Flocs are clearly far more complex in structure and behaviour and, therefore, it is important that the impacts of these features of flocs are understood in order that their settling behaviour can be assessed and so predicted with accuracy.

Floc aggregation is a dynamic process where mass, surface area, number, and morphology change as functions of the shear stress and time. Furthermore, whilst aggregates may have the same size, they may exhibit different structures due to different particle arrangements during aggregation.

65 The variations in mass, surface area and concentration substantially affect floc behaviour,
66 particularly with regard to collision and to aggregation efficiency (Vahedi & Gorczyca 2012).
67
68 Therefore, the irregular shape and porous structure of fractal aggregates may oppose the predicted
69 settling rate using solid spheres. These traits may affect aggregates density and porosity, and so the
70 drag forces on floc surface, making velocities (and hydraulic loading rates) slower than the ones
71 predicted by Stokes' law (Chakraborti and Kaur, 2014; Vahedi and Gorczyca, 2012). This may
72 potentially influences on the predicted clarification efficiency of settling units, resulting in quite
73 more solids dragged out from the tank into the subsequent filters, which may not be designed for
74 such extra load. Hence, the correct prediction of aggregates settling rates is crucial for the accurate
75 design of sedimentation tanks and subsequent filters in a full-scale water treatment plant.
76
77 Fractal geometry has been extensively used to characterise non-uniform objects and its application
78 on sedimentation will be described below, after a brief description of its main characteristic.
79
80 **Fractal geometry**
81 Fractals may be described as objects that demonstrate self-similarity (i.e. the existence of the same
82 pattern irrespective of viewing magnification). They can be expressed via a power law relationship
83 comprising two variables, and characterised by non-integer fractal dimensions, as shown in
84 Equation 1 to 3.
85 $$A \propto L^{D_f} \quad (1)$$
86 and:
87 $$V \propto A^{D_f} \quad (2)$$

where V, A and L refer to fractal volume, area and length respectively, whilst D_f is the floc fractal dimension.

In the case of flocs:

$$M \propto L^{D_f} \quad (3)$$

where M refers to floc mass.

Gregory (2009) described flocs as mass fractal objects and found that their fractal structure has important practical implications for floc density. Indeed, several factors affect flocs' fractal structure, including mixer device (Logan & Kilps 1995) and coagulation (Xu *et al.* 2010, 2011), as floc strength is a function of the formation process (He *et al.* 2012). Gregory (2009) found that aggregates formed by perikinetic flocculation display lower fractal dimension than those formed during orthokinetic flocculation, whilst aggregates formed during sweep coagulation are of larger size and fractal dimension compared with those formed during charge neutralization (Li *et al.* 2006, Kim *et al.* 2001).

Fractal aggregates, when densely compacted, are close to Euclidean objects and so have a large fractal dimension ($D_f \sim 2$, for two-dimensional objects), whereas smaller fractal dimensions result from highly branched structures. It is believed that these more compact aggregates, rather than those exhibiting large overall size, exhibit enhanced performance during sedimentation given that the floc settling velocity depends on the aggregate size and fractal dimension (Johnson, Li and Logan 1996; Gregory 1997; Chakraborti *et al.* 2000; Vahedi & Gorczyca 2012), as shown in Equation 4.

$$v_{st} = \frac{1}{18}\theta g \frac{\rho_p - \rho_w}{\mu} d_{50}^{3-D_f} \frac{d^{D_f-1}}{1+0.15\mathrm{Re}^{0.687}}\phi \quad (4)$$

where: v_{st} is the settling velocity of an individual floc; g is acceleration due to gravity; μ is dynamic viscosity of water; D_f is the fractal dimension; d is floc size; d_{50} is the median size of particles within floc (i.e. primary particles); θ is a dimensionless particle shape factor; ρ_p and ρ_w are the densities of primary particles and water, respectively.

$\phi = \frac{m_3}{m_f^{3/D_f}}$ and represents the size distribution of N primary mono-sized particles of diameter d_p in floc, as shown in Equations 5 and 6,

where:

$$m_3 = \left(\sum_{i=1}^{N} {d_p}_i^{\,3}\right)/N \quad (5)$$

and:

$$m_f = \left(\sum_{i=1}^{N} {d_p}_i^{\,D_f}\right)/N \quad (6)$$

The particle Reynolds, number, is given by Equation 7.

$$\mathrm{Re} = \frac{v_{st} d}{\upsilon} \quad (7)$$

where: ν is kinematic viscosity of water.

Bache *et al.* (1999) found that the floc effective density (ρ_e), given by $\rho_e = \rho_e - \rho_w$, is related to floc size (d) via Equation 8.

$$\rho_e = A d^{-n} \quad (8)$$

where: A is a packing factor and is a function of coagulant dose and coagulation pH; and n is a coefficient that is a function of D_f. For aluminium floc and humic substances, the value of n varies from 1.8 to 2.0.

Considering the importance of structural and morphological characteristics of fractal aggregates, the objective of the work reported in this paper is to investigate the porosity and density of aggregates after flocculation based on their fractal dimension calculated individually, measured by a non-intrusive image analysis based method, in order to inform our understanding of floc sedimentation and so improve clarification performance.

Methods

Suspensions

Suspensions were prepared in the laboratory from a kaolinite solution following Yukselen & Gregory (2004) to obtain a turbidity of 25 NTU. The kaolinite was characterized by scanning electron microscopy (SEM) using a JEOL JSM-6010LA microscope coupled to an X-ray spectrometer and via laser granulometry using the Malvern Mastersizer 2000 to obtain composition and mean grain size. The suspension was coagulated with commercial aluminium sulphate, and the pH was adjusted with a 1 M sodium hydroxide solution. The optimum coagulation conditions identified by Oliveira *et al.* (2015) using the same synthetic water were adopted, i.e., 2 mg $Al^{+3}.L^{-1}$, pH 7.5. Flocculation was performed with mean velocity gradients ($\overline{G_f}$) of 20 - 60 s^{-1}, which were determined by torque measurements, for flocculation times of 15 min to obtain flocs of different sizes and shapes.

Data Acquisition

1000 floc images were captured immediately post-flocculation (high-speed Miro EX-4 camera with interchangeable lenses, sampling at 25 Hz for 40 s). Image resolution was 800 x 600 pixels with a visual field of 6 x 8 mm. Shutter speed was set to 800 μs and pixel size was 10 μm. Illumination

was via a collimated laser beam modified by a cylindrical lens for plane dispersion with a thickness of 2 mm (following Moruzzi *et al*. 2017) placed perpendicular to the focus direction. Nominal laser power was 2000 mW, producing light at a wavelength of 532 nm (green). A schematic of the experimental apparatus is shown in Figure 1.

Digital images were processed using Image Pro Plus 7.0 software. The images were transformed into binary matrices by the segmentation process using a degree of 128/256 as the threshold and were then subjected to the particle image velocimeter (PIV) processing of the same package. Area and Diameter (max) of each floc were used to track each aggregate, with cut-off values of 200 pixels respectively (Chackraborti *et al.*, 2003). In total, 118 aggregates were selected, for which the attributes of interest (Diameter (max.), Diameter (min.), Diameter (mean), Area, Y coordinate, and Perimeter) were obtained. Further details on data acquisition and treatment can be found in Moruzzi *et al.* (2017, 2019).

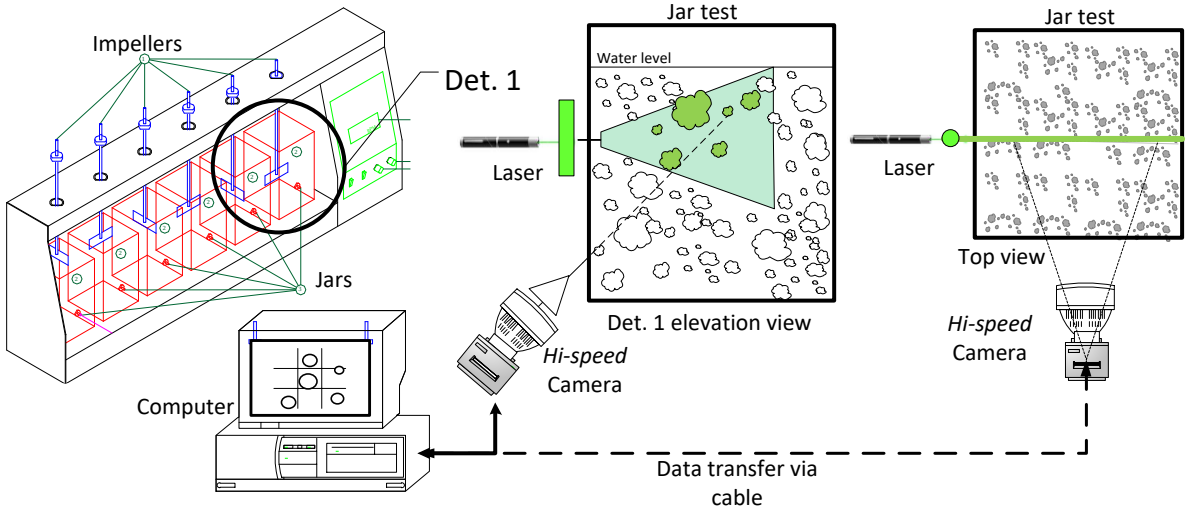

Figure 1 - Scheme of the experimental apparatus. Adapted from Moruzzi et al. (2017).

Determination of fractal characteristics

The value of D_f and the shape parameter, b, for each aggregate can be obtained from linear regression of the experimental data in the linearized form of Equation 9 (i.e. equation 10). Here, the slope of the straight line corresponds to the exponent (D_f) and the intercept corresponds to the shape parameter b.

$$N = b\left[\frac{d_f}{d_p}\right]^{D_f} \quad (9)$$

$$\ln N = \ln b + D_f \ln\left[\frac{d_f}{d_p}\right] \quad (10)$$

where: D_f is the three-dimensional fractal dimension; d_p is the primary particle diameter (m); d_f is the floc diameter (m); N is the number of primary particles of diameter d_p per volume of floc of diameter d_f; b is the shape parameter, defined as:

$$b = \left(\frac{\zeta.\xi}{\xi_0}\right)^{D_f/3} \quad (11)$$

where: ζ is the packing factor; ξ is the shape factor; ξ_0 is the primary particle shape factor.

The number of primary particles per unit of aggregate volume, N, was determined by rotation of the ellipsoid about the x-axis of the ellipsoid fitted to the highest and lowest dimensions determined by the image analyses, as illustrated in Figure 2 and Equations 12 and 13, following Chackraborti *et al*. (2000).

$$E = \left\{(x,y,z)\epsilon\mathbb{R}^3 : \frac{x^2}{a^2} + \frac{y^2}{b^2} + \frac{z^2}{c^2} \leq 1, a > 0, b > 0\ e\ c > 0\right\} \quad (12)$$

$$V(E) = \iiint_E \left(\frac{\partial A}{\partial x} + \frac{\partial B}{\partial y} + \frac{\partial C}{\partial z}\right) dx.dy.dz = \iint_S z dx dy \quad (13)$$

where: A, B, and C are the integration limits of the a, b, and c axes of the ellipsoid (E) with volume V(E); S is the surface of the ellipsoid (E).

193 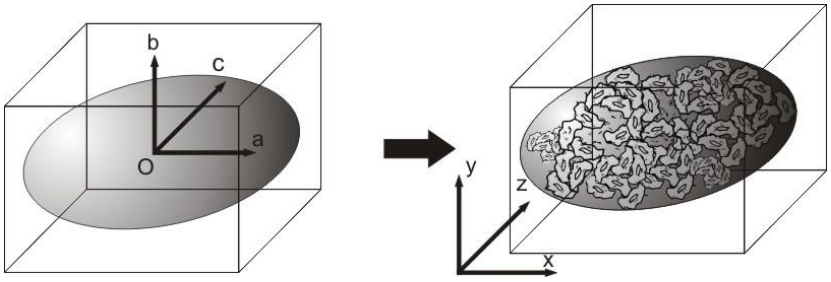

194 Figure 2 - Example of aggregate encased in ellipsoid

195 With these data, the value of the three-dimensional fractal dimension (D_{fp}) was obtained for the set
196 of aggregates by fitting the volumes to Equation 14 in the linearized form.

197

198 $$V \sim d_{max.}^{\ D_{fp}} \quad (14)$$

199 where: V is the volume of the ellipsoid containing the floc (m^3); $d_{max.}$ is the largest dimension of
200 the floc (m).

201

202 The two-dimensional fractal dimension (D_{fp}') for the set of aggregates was determined using
203 Equation 15, and the ratio of D_{fp} : D_{fp}' for the data set was then used to calculate the three-
204 dimensional fractal dimension per aggregate according to Equation 16. The value of d_p in Equation
205 16 was assumed from kaolin volume distribution, adopting mono-size primary particles as
206 simplification for the D_f calculation.

207 $$A \sim d_{max.}^{\ D_{fp}'} \quad (15)$$

208 where: A is the projected floc area on the image plane; D_{fp}' is the two-dimensional fractal
209 dimension.

210

211 $$D_f = \frac{D_{fp}}{D_{fp}'}\left(\frac{\ln N}{\ln\left(d_{max}/d_p\right)}\right) \quad (16)$$

With the shape, floc dimension, particle dimension, and three-dimensional fractal dimension parameters calculated per particle, the floc porosity and density were determined with Equations 17 and 18, considering a mass balance between the floc, the particle, and the voids occupied by the liquid.

The porosity of the floc, ε_f, with diameter d_f was determined via:

$$\varepsilon_f = 1 - \left(b.{d_f}^{D_f-3}.{d_p}^{3-D_f}\right) \quad (17)$$

and the floc density, ρ_f , via:

$$\rho_f = \rho_l + \left(b.{d_f}^{D_f-3}.{d_p}^{3-D_f}\left(\rho_p - \rho_l\right)\right) \quad (18)$$

Where: $\rho_f$is the floc density (kg.m^{-3}); ρ_l is the density of water (kg.m^{-3}); ρ_p is the density of the primary particle (kg.m^{-3}).

Settling velocity

The density, floc porosity, and three-dimensional fractal dimension were used to evaluate the sedimentation velocities of Euclidean geometry spheres (V_{sphere}) and fractals ($V_{fractal}$). It was assumed that the floc dimensions did not change during sedimentation. For this purpose, the Newton equation (Equation 19) in equilibrium ($\Sigma F_y=0$) was used for the particular case where the dimensionless Reynolds number (Re) < 1, such that the drag coefficient can be described according to Equation 20. Thus, V_{sphere} can be described by Equation 21 and $V_{fractal}$ by Equation 22, and they distinguish each other in the geometric and density terms of the Equations. The geometric term of

Equation 22 will always reduce the contribution of size on velocity for fractal aggregates, unless d_f approaches to d_p (for $d_f > d_p$) results in the square relation of Equation 21 (d_f^2). Finally, the ratio of the velocities was determined for each particle according to Equation 23.

$$V_{sphere} = \sqrt{\frac{4.(\rho_f - \rho_l).g.d_f}{3.\rho_l.C_d}} \quad (19)$$

where: V_{sphere} is the Newton velocity for the Euclidean sphere (m.s^{-1}); g is the acceleration due to gravity (m.s^{-2}); C_d is the drag coefficient.

Assuming Re<1,

$$C_d = \frac{24}{Re} = \frac{24\mu}{V_{st} d_f \rho_l} \quad (20)$$

where: Re is the Reynolds number; V is the floc terminal velocity (m.s^{-1}); μ is the absolute viscosity (N.m^{-2}.s).

Hence:

$$V_{sphere} = \frac{g(\rho_f - \rho_l) d_f^2}{18\mu} \quad (21)$$

Valid for Re< 1 and d_f < 1 mm.

$$V_{fractal} = \frac{g(\rho_p - \rho_l) d_f^{D_f - 1} d_p^{3 - D_f}.b}{18\mu} \quad (22)$$

where: $V_{fractal}$ is the velocity based on fractal aggregates with diameter d_f (m.s^{-1}).

The dimensionless quotient of the fractal and Euclidean sphere velocities, Γ, is defined as:

$$\Gamma = \frac{V_{fractal}}{V_{sphere}} \quad (23)$$

Results and discussion

Figure 3 shows the kaolinite (Kaolin, Fluka) particle size distribution: 0.4 – 100 μm, in volume with median 7.5 μm and in number (N) with median 1.0 μm, which is in agreement with other studies (Zbik & Smart 1998, Aparicio *et al.* 2004). An example of one scanning electron microscopy image taken from the kaolin dry sample is also presented in detail, showing qualitatively the range of size, shapes and textures of the primary particles. This result supports the definition of the appropriate pixel size for the determination of the smaller cluster of the aggregate, and primary particle size adopted herein as well.

Figure 4 shows a post flocculation (G_f = 20 s^{-1}, T_f = 15 min) aggregate characterization image. It is clear that any assumption of solid sphericity, and hence use of traditional Stokes' law approach is inappropriate for representing the shape of aggregates. Further, the existence of voids within the floc alters the porosity and density of the aggregate, both of which affect floc terminal velocity.

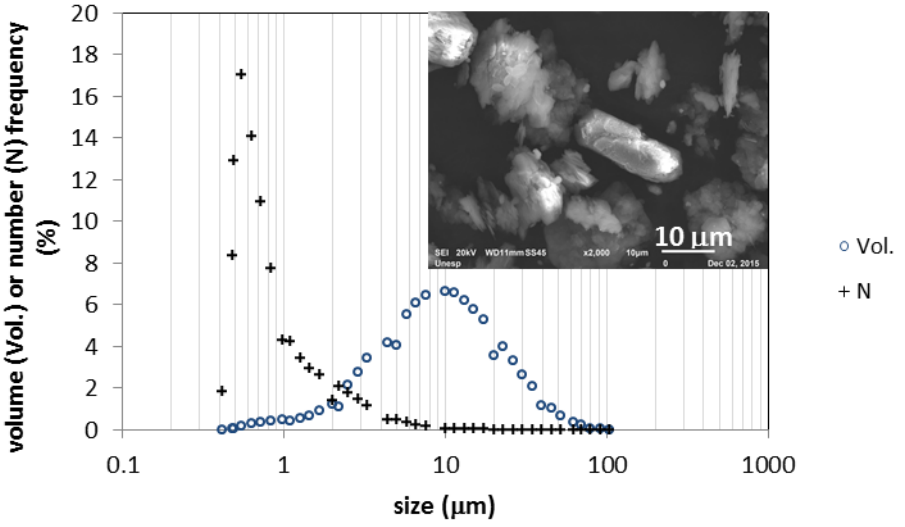

Figure 3 - Kaolin size distribution in number and volume. Scanning electron microscopy (SEM) image detail in the right upper side.

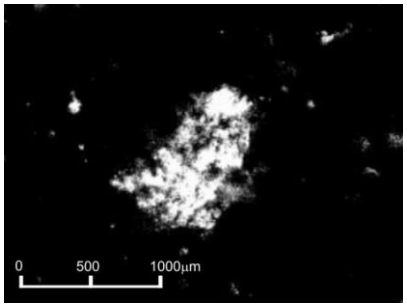

Figure 4 - Example of a porous aggregate image taken during sedimentation.

Figure 5 shows the relationship between log volume of the encased ellipsoid and the log of the ratio of $d_{max}:d_p$, from which the values b = 0.78 and D_{fp} = 2.35 were determined (Equation 10). The value of D_{fp} represents elongated medium aggregates, far from a perfect sphere, and agrees with other studies (Johnson, Li and Logan 1996; Chackraborti *et al.* 2003; Li *et al.* 2006). Plotting log aggregate area against log (d_{max}/d_p) yielded a 2-d fractal dimension, D_{fp}', value of 1.50. (Figure S.I.1).

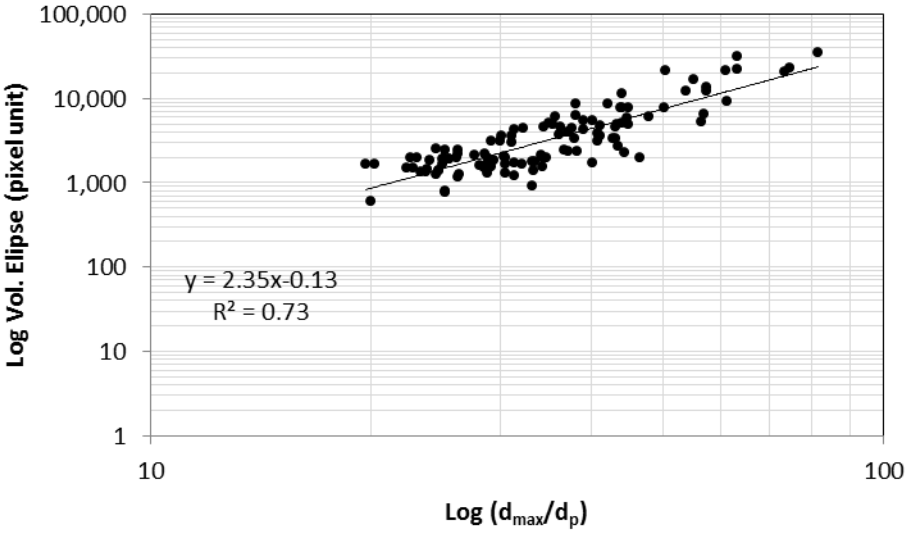

Figure 5 – Determination of three-dimensional fractal dimension from image analysis measurements by means of *log-log* plot of volume versus relative longest length based on pixel size.

285 These results were then applied to Equations 16, 17, and 18 to determine the three-dimensional
286 fractal dimension, porosity and density for the flocs.
287
288 Table 1 presents descriptive statistics obtained from all the aggregates in terms of the highest
289 dimension ($D_{max.}$), lowest dimension ($D_{min.}$), mean dimension (D_{mean}), aggregate fractal dimension
290 (D_f), porosity (ε), sphericity (Ψ) and density (ρ). Results show that the mean of the flocs' highest
291 dimension (D_{max}) was 362 μm, with a maximum of 816 μm, a standard deviation of 121 μm, and a
292 confidence interval (0.05) of 21 μm. For the flocs' lowest dimension (D_{min}), a mean of 138 μm
293 was obtained, with a maximum of 310 μm, a standard deviation of 47 μm, and a confidence interval
294 for the mean (0.05) of 8 μm. The average floc size obtained in the experiments was 231 μm, with
295 a maximum of 451 μm, a standard deviation of 70 μm, and a confidence interval for the mean
296 (0.05) of 12 μm. The three-dimensional fractal dimension (D_f) calculated per aggregate has a mean
297 of 2.61 for the interval [2.33 to 2.83], indicating a variety of floc shapes, ranging from the most
298 elongated to those close to spheres, in the limits of the interval. For the experiments, density was
299 obtained for the flocs (ρ_{floc}) with a mean of 1068 kg.m^{-3} within the range of [1024 to 1138 kg.m^{-3}].
300 The mean porosity (ε) of the aggregates was 0.76 with an interval of [0.53 to 0.91]. Sphericity (Ψ)
301 and aspect ratio (D_{max} / D_{min}) of 0.58 and 2.62 average, respectively, have shown that flocs are
302 majority elongated structures, far from spherical.
303 Figure 6 shows the relationship between porosity and fractal dimension, with the more open
304 structures (D_f<2.5) having a greater porosity (>80%) than more closed structures. To a lesser extent
305 than shape, large size flocs have also shown greater porosity for the same fractal dimension. The
306 average porosity found here (approximately 76%) is in agreement with Gorczyca & Ganczarczyk
307 (1999) and Vahedi & Gorczyca (2012) for large flocs. There is no doubt that shape and porosity

are dependant floc traits which may affect settling rate, however the nonhomogeneous mass distribution and pore population within aggregate structure are also important for terminal velocity, and should be considered for further developments, as suggested by Vahedi & Gorczyca (2014).

Table 1 – Descriptive statistic for aggregates' highest dimension ($D_{max.}$), lowest dimension ($D_{min.}$), mean dimension (D_{mean}), fractal dimension (D_f), porosity (ε), sphericity (Ψ), aspect ratio (D_{max} / D_{min}) and density (ρ).

Attribute	Average	Standard Deviation	Max	Min	95%*
D_{max} (μm)	362	121	816	196	21
D_{min} (μm)	138	47	310	73	8
$D_{average}$ (μm)	231	70	451	156	12
D_f (-)	2.61	0.09	2.83	2.33	0.02
ρ_f (kg m^{-3})	1068	22	1138	1024	4
ε (–)	0.76	0.07	0.91	0.53	0.01
Ψ (–)	0.58	0.14	0.97	0.14	0.02
D_{max} / D_{min}	2.62	0.67	5.14	1.53	0.12

* 95% significance

The direct consequence of the shape and porosity relation on flocs settling rates is the influences on an aggregate's density and drag. Unless water can flow through flocs voids, reducing resistance to settle, an elongated aggregate is more likely to have lower settling rates than those ones closer to a sphere-shape. The so called flow-through effect is still not well understood and there is also no consensus on the contribution of permeability for terminal velocities of porous aggregates.

Whilst initially Adler (1983) showed that the effect of permeability on flocs settling is minor and that is unlikely water can flow through pores during sedimentation. Nevertheless, Johnson et al. (1996) showed the more porous the floc is, the more likely fluid can flow through it, increasing permeability and so reducing resistance to settle. In general, literature has shown that elongated aggregates are likely to settle at lower rates than spheres and, according to Bushell et al. (2002), it is difficult to explain the greatly reduced resistance to settle described by Johnson et al. (1996).

Figure 7 shows that more spherical; less elongated aggregates (with increased D_f values) display a greater density, contributing to higher terminal velocity of aggregates. Therefore, the density of the aggregates varies inversely with porosity. If the mass was the predominant effect on floc settling velocity, compact spheres would always exhibit higher settling velocities. In fact, several researchers have shown that fractal aggregates can settle with slower velocities than those predicted by Stoke's law (Vahedi & Gorczyca, 2012; Tambo, 1979; Khelifa & Hill, 2006; Jarvis, et al., 2008).

Consequently, terminal velocities of aggregates will mostly depend upon the dual effect of porosity and density, determined to a great extent by aggregate shape, i.e fractal dimension.

Based on the experimental results, it was possible to construct a relationship between porosity (ε) and the density (ρ_f) of the aggregate (S.I. Figure 2, and Equations 24 and 25) such that:

$$\varepsilon = A(1 - B\rho_f) \quad (24)$$

where:

$$A = \left(1 - \frac{\rho_l}{\rho_p}\right)^{-1} \quad (25)$$

$$B = {\rho_p}^{-1}$$

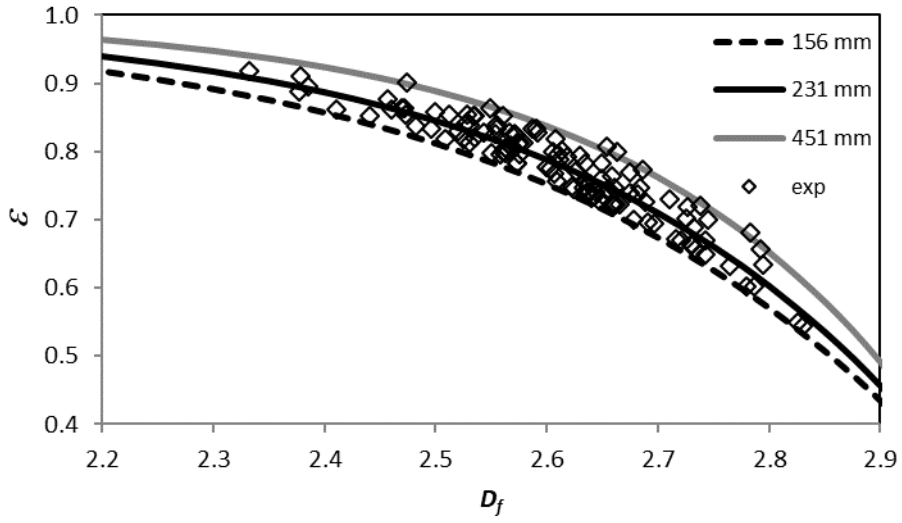

344

345 Figure 6 –Aggregates porosity ε (–) as a function of D_f for the minimum, average and maximum

346 aggregate size in micrometer (μm).

347

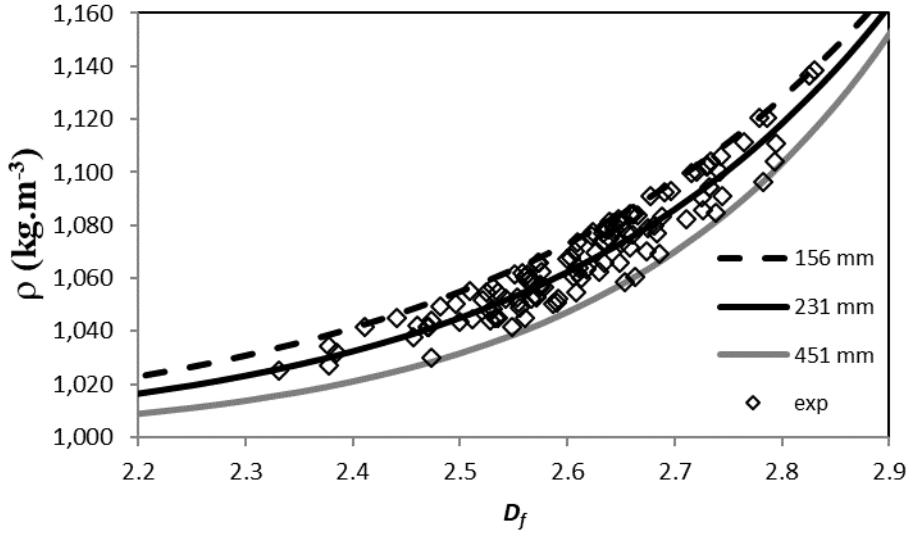

348

349 Figure 7 – Density of the aggregates ρ_f as a function of D_f for the minimum, average and maximum

350 aggregate size in micrometer (μm).

351

352 Common practice for designers of sedimentation tanks is to adopt average floc density for perfect
353 spheres, so that settling velocities of aggregates can be simulated using a characteristic aggregate
354 size and Stokes's law, as Equation 21. However, results shown here suggest that flocs are
355 elongated, porous structures, and far from spherical.
356
357 The impact of this oversimplification of floc shape is that the drag force changes as result of the
358 cross-section area, thus altering the settling velocity. In general, it is supposed that deviation from
359 sphericity will result in increasing drag, irrespective of floc orientation and permeability (Bushell
360 et al., 2002). However, Johnson et al. (1996) suggest that the actual drag is lower than that
361 calculated for fractal aggregates, even when permeability is considered. Figure 8 shows calculated
362 settling velocity for spheres and flocs (based on Equations 21 and 22 for d_p of 7.5 μm, this being
363 median particle size by volume) against floc size for different shapes, i.e. fractal dimensions (D_f =
364 3.00 for spheres; 2.33, 2.61 and 2.83 for fractals).
365
366 Figure 8 shows that fractal aggregates of size between 100 and 300 μm settle with velocities
367 between 0.3 and 7.9 mm/s, which is in agreement with results presented by Vahedi & Gorczyca
368 (2012), Khelifa & Hill (2006) and Jarvis *et al*. (2008), who performed both experiments and
369 simulations. The authors showed settling velocities varying from 0.1 to 7.1 mm/s for aggregate size
370 between 100 and 300 μm, corroborating that the simulations presented here are within experimental
371 measurements performed by several authors. Nevertheless, results compiled by Khelifa & Hill
372 (2006) reveal there is considerable scatter in settling velocity of fractal aggregates, varying up to
373 100 fold each other for the same floc size, possibly due to the nonhomogeneous mass distribution
374 and pore population mentioned by Vahedi & Gorczyca (2014). Here, aggregates with a fractal

375 dimension of 2.83 settled with higher velocities than spheres of same size, for all range of floc
376 sizes, due to the usual assumption that spherical flocs have the same density as fractal aggregates,
377 and so less mass than aggregates of equal size.
378
379 Conversely, for aggregates with fractal dimension of 2.33 and 2.61 there is a size threshold above
380 which fractals settle with lower velocities than those calculated using Stokes' law for compact
381 spheres. For small floc sizes, close to the size of primary particle ($d_f \approx d_p$), the geometric term of
382 Equation 22 approaches to the term d_f^2 from Equation 21 and, therefore, the differential density
383 between particle and liquid is the predominant driving effect over settling rate, surpassing the
384 reduction caused by the fractal geometry. However, the differential density is not enough to surpass
385 the reduction in the geometry term of Equation 22, caused by the low fractal dimension of elongated
386 large aggregates. Results presented by Vahedi & Gorczyca (2012) have also shown that multi
387 fractal aggregates can settle with lower velocities than those predicted by modified Stokes' law, by
388 introducing a porous effect into the original equation. The authors simulated fractal aggregates with
389 multi fractal dimension varying from 2.6 to 2.7 and aggregates size less than 320 μm. In contrast,
390 experiments carried out by Johnson *et al.* (1996) showed that settling velocities of fractal
391 aggregates were between 4 and 8 times greater than those predicted by Stokes' law, for aggregates
392 size in the range of 100 to 1000 μm. Here, fractal aggregates (D_f = 2.61, d_f > 320 μm) settle with
393 lower velocities than those predicted by Stokes' law; whilst, for D_f = 2.33, all aggregates of d_f > 70
394 μm and d_p = 7.5 μm settled below the velocity calculated by Stokes' law for spheres.
395
396 The ratio of the fractal to Euclidean velocities (Γ) is shown in Figure 9-a for different values of the
397 aggregates' mean equivalent diameter (d_f) in the situation (D_f = 3.00 for spheres; 2.33, 2.61 and

2.83 for fractals). The ratio of fractal aggregate to sphere settling velocity (the former being obtained from fractal porosity and density considerations), varied from 0.16 to 4.11 for aggregates in the range of 10 and 1000 μm, primary particle size of 7.5 μm and three-dimensional fractal dimension between 2.33 and 2.83. This emphasizes that fractal aggregates can behave differently, settling with higher or lower velocities, compared to Stokes' law, once settling velocities of aggregates depend upon the dual effect of porosity and density, determined by the aggregate's shape. Although large elongated flocs contain higher mass their shape results in lower contribution of geometric term of Equation 22 over settling rate than small flocs. This would only be overcome whether water could flow through flocs' pores whilst settling, as a result of macro pores distribution within aggregates, as mentioned by Vahedi & Gorczyca (2012). Again, there is no consensus about the permeability effect on settling rate of fractal aggregates, and despite the fact that permeability was not considered here for modelling, the findings are in agreement with a wide range of experiments, like those performed by Vahedi & Gorczyca (2012) and Johnson, Li and Logan (1996), for instance.

On the other hand, if primary particle size is changed, results vary for the same fractal geometry. Figure 9-b shows the effect of primary particle size (d_p) on Γ. Results were taken following the same procedures used for Figure 9-a, and it is clear that the d_p of 1.0 μm can change the ratio of fractal aggregate to sphere settling velocity markedly to values between 0.04 to 2.92, i.e. in a lower range when compared to d_p of 7.5 μm. For the same fractal dimension, the lower d_p the higher the porosity and, therefore, the lower the density thus affecting the mass contribution over terminal velocities of aggregates. Further, results showed all velocities simulated for fractal dimension of 2.33 were far lower than those predicted by Stokes' law for spheres ($\Gamma < 1$), and only aggregates

421 with size lower than 40 μm settled with higher velocities than Stokes' law for spheres when fractal
422 dimension of 2.61 was simulated; although, Γ was always higher than 1 for fractal dimension of
423 2.83.
424
425 Whether lower or higher, simulations have shown that settling velocities of fractal aggregates can
426 be far different from those predicted by spheres using Stokes' law. The factors affecting settling
427 velocities of fractal aggregates depend upon size, shape, porosity, permeability, primary particle
428 size, and are far more complex than assumed by Stokes' law for spheres. Results presented in this
429 paper have shown that settling velocities may vary strongly when floc shape changes from spherical
430 to fractal aggregates, and the accuracy of predictions varies with floc size, fractal dimension and
431 primary particle size. In practice, settling velocities of flocs are a function of floc size and fractal
432 dimension, which are controlled by coagulation flocculation units.

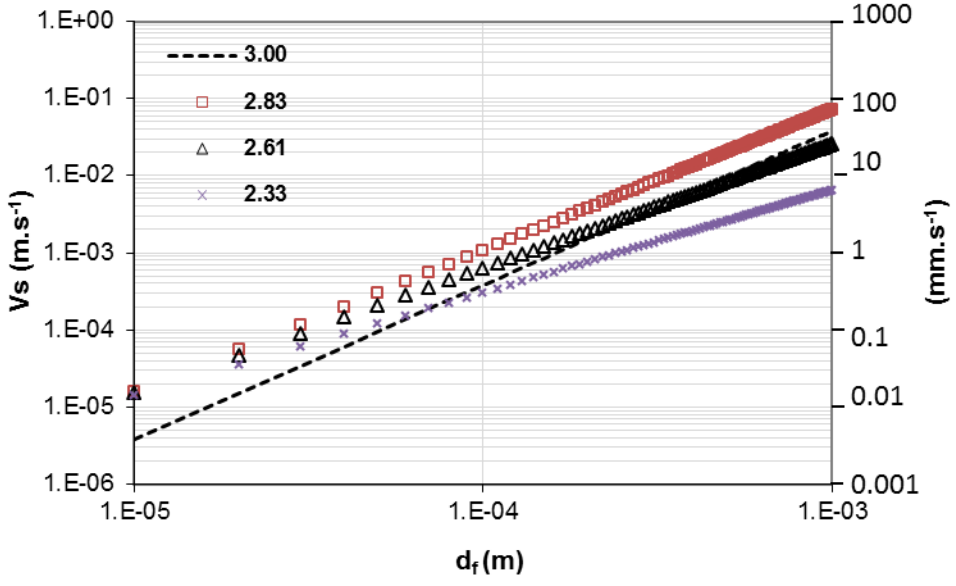

433

434 Figure 8 – Simulation of terminal velocities for Euclidean sphere (D_f of 3 and ρ_f of 1068 kg.m^{-3})
435 and fractal (D_f of 2.83, 2.61 and 2.33).ρ_l of 998 kg.m^{-3}. d_p of 7.5 μm.

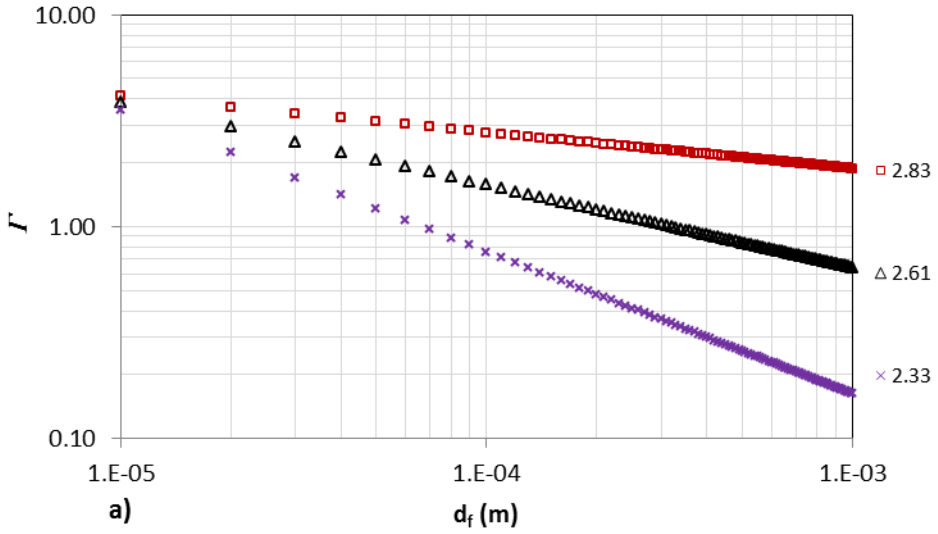

436

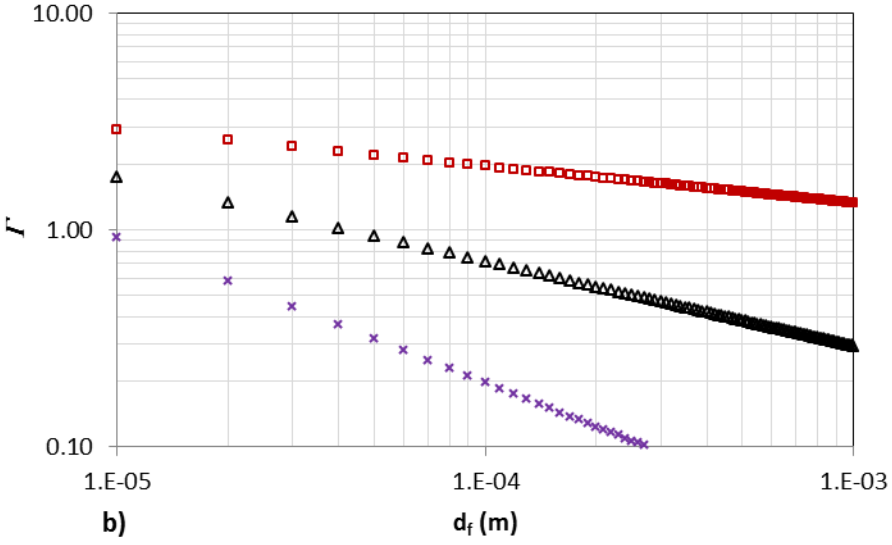

437

438 Figure 9 - Fractal to Euclidean velocities ratio (Γ) for D_f of 2.83, 2.61 and 2.33. (a) d_p of 7.5 μm

439 (b) d_p of 1.0 μm.

440

441 **Conclusions**

442 In this study, the porosity and density of aggregates formed after the flocculation of water

443 containing kaolin were calculated using fractal dimension, and the terminal velocities of the

444 Euclidean sphere and of the fractal aggregates were determined using images of a series of 118
445 flocs measured individually.
446
447 Settling has not been used as a means to characterise aggregates behaviour, but image analysis
448 instead. Therefore, simulations here performed derived from aggregates' characteristics taken by
449 image analysis, to input data into both the Stokes' equation and the modified equation, based on
450 fractal geometry. Findings are in agreement with a wide range of aggregates traits and setting rates
451 reported in literature, confirming that results are reliable.
452
453 A consistent increase of aggregate porosity with decrease of fractal dimension was observed, and
454 the opposite was observed for density of aggregates. Therefore, more spherical aggregates display
455 a greater density, contributing to higher terminal velocity of aggregates.
456
457 It was found that fractal aggregates can behave differently, settling with higher or lower velocities,
458 compared to Stokes' law, once settling rates of aggregates depend upon the dual effect of porosity
459 and density, determined by the aggregate's size and shape. For small floc sizes, close to the size of
460 primary particle ($d_f \approx d_p$) the differential density between particle and liquid is the dominant effect
461 on settling rate, surpassing the geometry reduction yielded by fractal aggregates. The opposite was
462 observed to large fractal aggregates, where the differential density was not big enough to surpass
463 the reduction caused by the low fractal dimension of elongated aggregates.
464
465 The results obtained differ from other work in the field by calculating settling velocities from fractal
466 dimension and demonstrated the importance of advancing the analysis of particles considering their

sizes and shapes beyond those described by Euclidean geometry. Specifically, applying fractal geometry to determine the porosity and density of the flocs is an important evaluation tool, with far-reaching implications for sedimentation tank design and operation.

Acknowledgments

Rodrigo B. Moruzzi is grateful to São Paulo Research Foundation (Fundação de Amparo à Pesquisa do Estado de São Paulo—FAPESP) Grant 2017/19195-7 for financial support and to CNPq for the fellowship Grant 301210/2018-7.

References

Adler, P. M. 1987. Hydrodynamic properties of fractal flocs. Faraday Discussions of the Chemical Society, **83**, 145-152.

Aparicio P., Pérez-Bernal J. L., Galán E. & Bello A. 2004 Kaolin fractal dimension. Comparison with other properties. *Clay Minerals*, **39**(1), 75-84.

Bache D. H., Rasool E., Moffatt D. & Mcgilligan F. J. 1999 On the strength and character of alumino-humic flocs. *Water Science Technology*, **40**(9), 81–88.

Becker V., Schlauch E., Behr M. & Briesen, H. 2009 Restructuring of colloidal aggregates in shear flows and limitations of the free-draining approximation. *Journal of Colloid and Interface Science*, **339**(2009) 362-372.

Bushell, G. C., Yan, Y. D., Woodfield, D., Raper, J. U. D. Y., & Amal, R. O. S. E. 2002. On techniques for the measurement of the mass fractal dimension of aggregates. *Advances in Colloid and Interface Science*, 95(1), 1-50.

Chakraborti R. K., Atkinson J. F. & Van Benschoten J. E. 2000 Characterization of alum floc by image analysis. *Environmental Science and Technology*, **34**(18), 3969–3976.

Chakraborti R. K., Gardner K. H., Atkinson J. F. & Van Benschoten J. E. 2003 Changes in fractal dimension during aggregation. *Water Research*, **37**(4), 873–883.

Gorczyca, B., & Ganczarczyk, J. E. R. Z. Y. 1999 Structure and porosity of alum coagulation flocs. *Water Quality Research Journal*, 34(4), 653-666.

Chakraborti RK, Kaur J. 2014 Noninvasive Measurement of Particle-Settling Velocity and Comparison with Stokes' Law. Journal of Environmental Engineering., 140(2):04013008.

Gregory J. 1997 The density of particle aggregates. *Water Science Technology*, **36**(4), 1-13.

Gregory J. 2009 Monitoring particle aggregation processes. *Advances in Colloid and Interface Science*, **147-148**, 109-123.

He W, Nan J, Li H. Y. & Li S. 2012 Characteristic analysis on temporal evolution of floc size and structure in low-shear flow. *Water Research*, **46**(2)**,** 509–520.

Jarvis, P., Parsons, S. A., Henderson, R., Nixson, N., & Jefferson, B. 2008 The practical application of fractal dimension in water treatment practice–the impact of polymer dosing. *Separation Science and Technology*, **43**(7), 1785-1797.

Johnson C. P., Li X. & Logan B. E. 1996 Settling velocities of fractal aggregates. *Environmental Science & Technology*, **30**(6), 1911-1918.

Khelifa, A., & Hill, P. S. 2006 Models for effective density and settling velocity of flocs. *Journal of Hydraulic Research*, **44**(3), 390-401.

509 Kim S. H., Moon B. H. & Lee H. I. 2001 Effects of pH and dosage on pollutant removal and floc
510 structure during coagulation. *Microchemical Journal*, **68**(2-3), 197-203.

511 Lawler D. F. 1997 Particle size distribution in treatment process: theory and practice. *Water Science*
512 *and Technology*, **36(**4), 15-23.

513 Li T., Zhu Z., Wang D., Yao C. & Tang H. 2006 Characterization of floc size, strength and structure
514 under various coagulation mechanisms. *Powder Technology*, **168**, 104-110.

515 Logan B. E. & Kilps B. E. 1995 Fractal dimensions of aggregates formed in different fluid
516 mechanical environments. *Water Research*, **29**(2), 443-453.

517 Moruzzi, R.B., Oliveira, A.L, Conceição, F.T, Gregory, J, Campos, L.C. 2017 Fractal dimension
518 of large aggregates under different flocculation conditions, *Sci. Total Environ.* 609, 807–814.

519 Moruzzi, R. B., da Silva, P. G., Sharifi, S., Campos, L. C., & Gregory, J. 2019 Strength
520 assessment of Al-Humic and Al-Kaolin aggregates by intrusive and non-intrusive methods.
521 *Separation and Purification Technology*, 217, 265-273.

522 Oliveira A. L., Moreno P., Silva, P. A. G., De Julio, M. & Moruzzi, R. B. 2015 Effects of the fractal
523 structure and size distribution of flocs on the removal of particulate matter. *Desalination and Water*
524 *Treatment*, **57**(36), 16721-16732.

525 Spicer P. T. & Pratsinis S. E. 1996 Shear-induce flocculation: the evolution of floc structure and
526 the shape of the size distribution at steady state. *Water Research*, **30**(5), 1049-1056.

527 Tambo, N. Watanabe, Y. 1979 Physical characteristics of flocs—I. The floc density function and
528 aluminium floc. *Water Research*, **13**(5), 409-419.

529 Veerapaneni, S., & Wiesner, M. R. 1996 Hydrodynamics of fractal aggregates with radially varying
530 permeability. *Journal of Colloid and Interface Science*, 177(1), 45-57.

531 Vahedi A. & Gorczyca B. 2012 Predicting the settling velocity of flocs formed in water treatment
532 using multiple fractal dimensions. *Water Research*, **46**(2012), 4188-4194.

533 Wu R. M., Lee D. J., Waite T. D. & Guan J. 2002. Multilevel structure of sludge flocs. *Journal of*
534 *Colloid and Interface Science*, **252**(2), 383–392.

535 Xu W., Gao B., Yue Q. & Wang Y. 2010 Effect of shear force and solution pH on flocs breakage
536 and re-growth formed by nano-Al_{13} polymer. *Water Research*, **44**(6), 1893-1899.

537 Xu W., Gao B., Yue Q. & Bo X. 2011 Influence of pH on flocs formation, breakage and fractal
538 properties — the role of Al_{13} polymer. *Journal of Water Sustainability*, **1**(1), 45-57.

539 Yang Z., Yang H., Jiang Z., Huang Z., Li H., Li A. & Cheng R. 2013 A new method for calculation
540 of flocculation kinetics combining Smoluchowski model with fractal theory. *Colloids and Surfaces*
541 *A: Physicochemical and Engineering Aspects*, **423**, 11-19.

542 Yukselen M. A., Gregory J. 2004 The reversibility of flocs breakage. *International Journal of*
543 *Mineral Processing*, **73**(2-4), 251-59.

544 Zbik M. & Smart, R. St. C. 1998 Nanomorphology of kaolinites: comparative SEM and AFM
545 studies. *Clays and Clay Minerals* **46**(2), 153-160.

546 SUPPLEMENTARY INFORMATION (S.I)

547

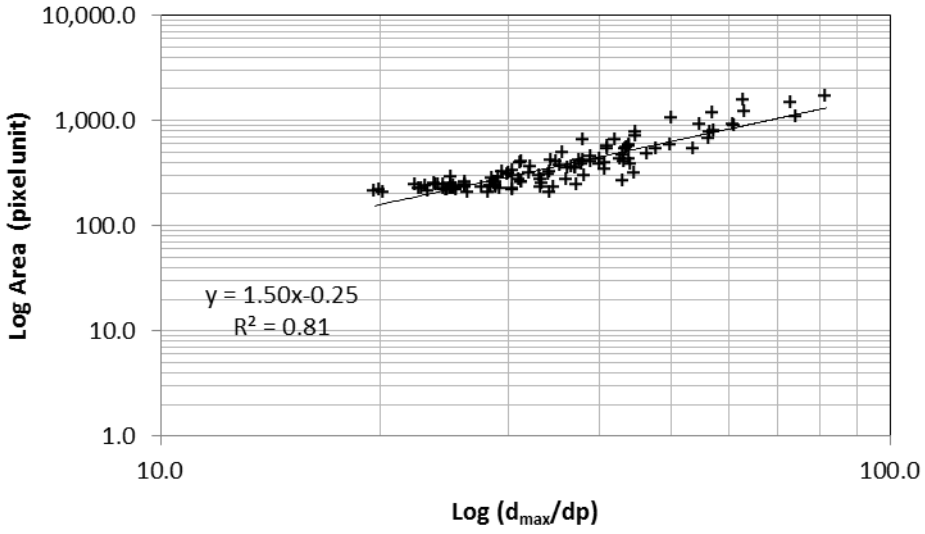

548

549 Figure S.I.1 –*log-log* plot of area versus relative longest length based on pixel size.

550

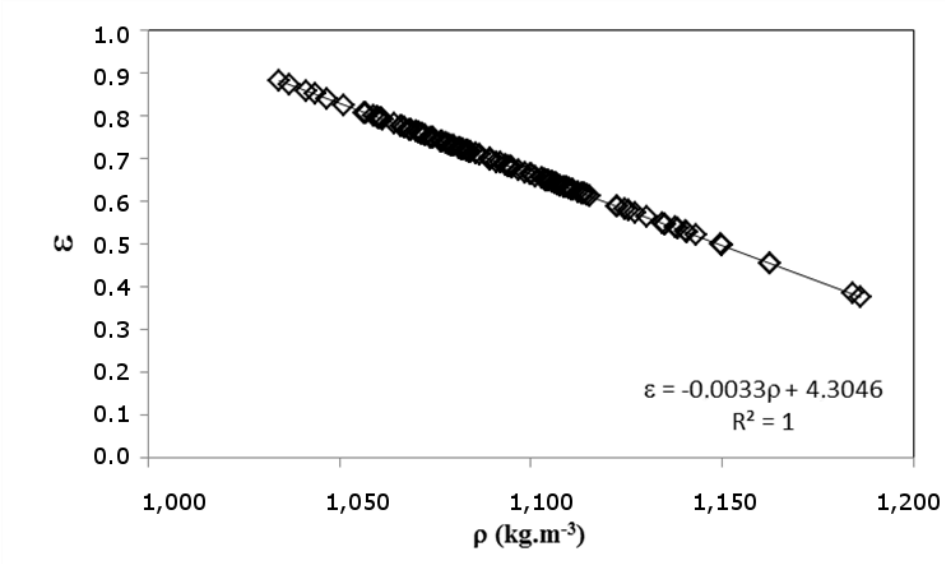

551

552 Figure S.I.2 – Aggregate porosity (ε) as a function of density.